Equalization Techniques for Multipath Mitigation in Aeronautical Telemetry

Michael Rice
Brigham Young University
Provo, UT 84602
mdr@ee.byu.edu

Ed Satorius
Jet Propulsion Laboratory
Pasadena, CA
Edgar.H.Satorius@jpl.nasa.gov

Abstract—**This paper describes the application of adaptive equalization based on the constant modulus algorithm (CMA) and the decision-directed minimum mean squared error (DF-MMSE) concept to the two compatible offset QPSK waveforms (FQPSK and SOQPSK-TG) that constitute the ARTM Tier-1 waveforms. An adaptive version of the DF-MMSE equalizer is developed and applied to this application. In the presence of frequency selective multipath interference typically encountered in aeronautical telemetry, both equalization techniques are shown to provide reliable performance for FQPSK and SOQPSK-TG. The performance of both waveforms with the DF-MMSE equalizer is slightly better than that using the CMA equalizer. Implementation trade-offs between the two types of equalizers are discussed.**

I. Introduction

The complexity of airborne military systems has increased dramatically over the past 40 years. As a result, the data rates required to test these systems has increased from 100 kbits/sec in the 1970s to 10-20 Mbits/sec today. The consequences of this trend are 1) spectral efficiency has become more important and 2) the multipath interference encountered in aeronautical telemetry has become frequency selective.

The spectral efficiency of PCM/FM, which has been the dominant carrier modulation in aeronautical telemetry for more than 40 years, has proven inadequate. The wide bandwidths required for high data-rate tests have applied tremendous pressure to the spectral allocations at L-band (1435 – 1535 MHz), lower S-band (2200 – 2290 MHz), and upper S-band (2310 – 2390 MHz). The situation was further exacerbated in 1997 when the lower portion of upper S-band from 2310 to 2360 MHz was reallocated in two separate auctions: 2320 – 2345 MHz was reallocated for digital audio radio in one round while 2305 – 2320 MHz and 2345 – 2360 MHz were allocated to wireless communications services in the subsequent rounds.

In response, the Advanced Range Telemetry (ARTM) program [1] was launched by the Central Test and Evaluation Investment Program (CTEIP) in 1997 to identify more bandwidth efficient modulation formats suitable for use in aeronautical telemetry. The goal was to select modulation schemes that required less bandwidth than PCM/FM, but had the same detection efficiency. The severe size and weight restrictions typical of these applications requires power amplifiers running full saturation or even class C amplifiers. As a consequence, the search has focused on constant envelope waveforms. New modulation formats were selected in two phases. In the first phase, a version of the Feher-patented QPSK (called, FQPSK-B) [2] was adopted in 2000 as part of the IRIG 106 standard [3]. A compatible variant of the MIL-STD 188-181 Shaped Offset QPSK (SOQPSK) [4] was selected as a compatible alternative in 2004. These two modulation formats, known collectively as the "ARTM Tier-1 Waveforms," have the same detection efficiency as PCM/FM but twice the spectral efficiency as PCM/FM [5], even when used with non-linear power amplifiers. In the second phase, a two index 3RC CPM modulation, described in [6], was selected as the "ARTM Tier-2 Waveform." This waveform, simply called "ARTM CPM" in the 2004 version of IRIG 106, has the same detection efficiency as PCM/FM and approximately 3 times the spectral efficiency of PCM/FM [7].

The second consequence of the increased data rates is the frequency selective nature of the multipath interference. The data links used in aeronautical telemetry are subject to multipath interference in the form of strong "ground bounces" (especially at low elevation angles) and reflections off irregular terrain [8]. At low data rates, such as 100 kbits/sec, the multipath interference appears as flat fading across the signal bandwidth. At high data rates, the signal bandwidth is much wider and the multipath interference is characterized by deep spectral nulls. The frequency selective nature of the multipath interference disrupts the data link and is the main cause of data loss in aeronautical telemetry.

Equalization has been applied as a multipath mitigation technique for several decades [9]. Adaptive equalizers are commonly used since they are able to track changes in the characteristics of the multipath interference. This paper summarizes an investigation into the performance of adaptive equalizers as a multipath mitigation technique for the ARTM Tier-1 waveforms. The ARTM Tier-1 waveforms are described in Section II and applicable equalization techniques are described in Section III. Adaptive equalizers based on the constant modulus algorithm (CMA) and the decision feedback minimum mean squared error (DF-MMSE) concept are presented. DF-MMSE equalization for offset modulations was developed by Tu [10]. This paper extends these concepts to an adaptive solution. In Section IV, the bit error rate performance of these equalizers is summarized. It is shown that both types

0-7803-8847-X/04/$20.00 ©2004 IEEE

of equalizers are able to provide reliable performance in the presence of multipath interference typical of that encountered in aeronautical telemetry. The bit error rate of both waveforms is slightly better with the DF-MMSE equalizer than with the CMA equalizer. The trade-offs between the two types of equalizers is discussed in Section V.

II. ARTM Tier-I Waveforms

A. FQPSK

Feher-patented QPSK (FQPSK) [11] is a variant of offset QPSK where the inphase and quadrature components of the modulated waveform are cross correlated to produce a quasi-constant envelope signal [12], [13]. Following Simon [13], the FQPSK waveform may be expressed in terms of a set of 16 baseband pulse shapes $S_m(t)$ for $m = 0, 1, \ldots, 15$. During the symbol interval $nT_s \le t \le (n+1)T_s$, the waveform $S_{i(n)}(t - nT_s)$ is used to amplitude modulate the inphase component of the carrier. Likewise, during the interval $(n + 1/2)T_s \le t \le (n + 3/2)T_s$, the waveform $S_{q(n)}(t - (n - 1/2)T_s)$ is used to amplitude modulate the quadrature component of the carrier. The indices $i(n), q(n) \in \{0, 1, \ldots, 15\}$ are determined by the input data streams as described in [13]. The complex baseband FQPSK waveform may be represented as

$$f(t) = \sqrt{E_b} \sum_n \left[S_{i(n)}(t - nT_s) + jS_{q(n)}(t - (n + 1/2)T_s) \right] \quad (1)$$

where E_b is the average bit energy and T_s is the symbol period (or reciprocal of the symbol rate).

The optimal detector is a sequence detector using a trellis that accounts for the possible combinations of waveforms determined by the memory of the waveform mapper [13]. In practice, symbol-by-symbol detection is used since this type of detector is compatible with generic offset QPSK and shaped-offset QPSK [3]. The symbol-by-symbol detector is illustrated in Figure 1. After rotation by the carrier phase synchronizer, the received waveform is filtered by a detection filter with impulse response $g(t)$. Integrate-and-dump detection is realized when $g(t) = 1$ for $0 \le t \le T_s$ and 0 otherwise. Simon [13] showed that use of a detection filter matched to the average of the 16 possible waveforms is approximately 1/2 dB better than the integrate-and-dump detection filter in the AWGN environment. (The trellis detector is about 1 dB better than the symbol-by-symbol detector using a detection filter matched to the average of the pulse shapes.)

B. SOQPSK-TG

Shaped Offset QPSK (SOQPSK) is a ternary CPM modulation format whose modulation index $h = 1/2$. Using complex baseband notation, the SOQPSK waveform may be represented as

$$s(t) = \exp\{j\phi(t)\} \quad (2)$$

$$\phi(t) = \pi \sum_k \alpha(k) g(t - kT_b) \quad (3)$$

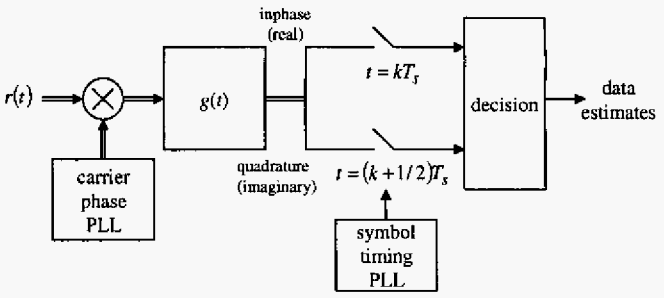

Fig. 1. Symbol-by-symbol detector for FQPSK and SOQPSK using a simple detection filter.

where $\alpha(k) \in \{-1, 0, +1\}$ is the k-th ternary symbol, T_b is the bit time, and $g(t)$ is a phase pulse that is the time integral of a frequency pulse $p(t)$ with area 1/2. The frequency pulse defined in MIL-STD 188-181 is a rectangular pulse with duration T_b and amplitude $T_b/2$. IRIG-106 specifies a more bandwidth efficient variation of this waveform which it terms SOQPSK-TG. The frequency pulse for SOQPSK-TG is a *spectral* raised cosine pulse that is been windowed by a *temporal* raised-cosine. The phase and frequency pulses for SOQPSK-TG are given by [4]

$$g(t) = \int_{-\infty}^{t} p(x)dx \quad (4)$$

$$p(t) = A \frac{\cos\left(\frac{\pi\rho Bt}{2T_b}\right)}{1 - 4\left(\frac{\rho Bt}{2T_b}\right)^2} \times \frac{\sin\left(\frac{\pi Bt}{2T_b}\right)}{\frac{\pi Bt}{2T_b}} \times w_n(t) \quad (5)$$

where the window is

$$w_n(t) = \begin{cases} 1 & 0 \le \left|\frac{t}{2T_b}\right| \le T_1 \\ \frac{1}{2} + \frac{1}{2}\cos\left(\frac{\pi}{T_2}\left(\frac{t}{2T_b} - T_1\right)\right) & T_1 \le \left|\frac{t}{2T_b}\right| \le T_1 + T_2 \\ 0 & T_1 + T_2 < \left|\frac{t}{2T_b}\right|. \end{cases} \quad (6)$$

and the constant A is chosen to make the area of $p(t)$ 1/2. The waveform is completely specified by the parameters ρ, B, T_1, and T_2. For SOQPSK-TG the values are[1] $\rho = 0.7$, $B = 1.25$, $T_1 = 1.5$, and $T_2 = 0.5$. The frequency pulse has support on the interval $-2 \le t/2T_b \le 2$ and thus spans 4 signaling intervals. SOQPSK-TG is an example of *partial response* CPM [14]. The mapping from bits to ternary symbols is described in [4].

The name "shaped offset QPSK" follows from the observation that each ternary symbol causes the carrier phase either advance by $\pm\pi/2$ radians or to remain at its current value. When viewed on an I-Q plot, the carrier phase appears

[1] In the original publication [4], two versions of SOQPSK were described: SOQPSK-A defined by $\rho = 1$, $B = 1.35$, $T_1 = 1.4$, and $T_2 = 0.6$ and SOQPSK-B defined by $\rho = 0.5$, $B = 1.45$, $T_1 = 2.8$, and $T_2 = 1.2$. SOQPSK-A has a slightly narrower bandwidth (measured at the -60 dB level) and slightly worse detection efficiency than SOQPSK-B. The Telemetry Group of the Range Commanders Council adopted the compromise waveform, designated SOQPSK-TG in 2003.

to migrate from quadrant to quadrant along the unit circle. By contrast, the carrier phase of (unshaped) Offset QPSK migrates from quadrant to quadrant instantaneously. Since the phase pulse "shapes" the phase trajectory of the carrier from what it would be for unshaped OQPSK, the waveform has an interpretation as a "shaped" OQPSK.

The use of a linear detector of the form illustrated in Figure 1 for use with binary CPM with $h = 1/2$ has been analyzed in [15], [16]. Detection filters for SOQPSK have been studied by Geoghegan, et. al [17] using experimental techniques.

III. Adaptive Equalizers for ARTM Tier-1 Waveforms

A. Equalization Based the Constant Modulus Algorithm

The equalizers based on the constant modulus algorithm (CMA) are special case of *blind* equalization techniques that do not require knowledge of the data symbols or timing synchronization. This class of equalization techniques for I/Q modulated waveforms seeks to minimize an error due to Godard [18] of the form

$$e(n) = E\left\{\left(|r(n)|^p - R_p\right)^2\right\} \tag{7}$$

where R_p is a constant that depends on the properties of the modulated waveform. The constant modulus algorithm, uses the special case $p = 2$ [19], [20]. The CMA is a natural choice for the ARTM tier-1 waveforms since the waveforms were selected, in part, because they have a constant envelope.

Since the CMA equalizer is blind, it may be "inserted" prior to the detector of Figure 1 as illustrated in Figure 2 (a). The received complex baseband waveform is sampled every T seconds to provide samples at a normalized rate of $N = T_s/T$ samples/symbol. The received sample $r(n)$ is processed by a length-L FIR equalizer filter to produce the output sample

$$y(n) = \sum_{l=0}^{L-1} w^{(n)}(l) r(n-l) \tag{8}$$

where $w^{(n)}(l)$ is the set of filter coefficients used at time index n. The modulus error at time step n is computed using

$$e(n) = \left(|y(n)|^2 - 1\right)^2. \tag{9}$$

This error is used in an LMS algorithm [21] to update the filter coefficients using

$$\begin{bmatrix} w^{(n+1)}(0) \\ w^{(n+1)}(1) \\ \vdots \\ w^{(n+1)}(L-1) \end{bmatrix} = \begin{bmatrix} w^{(n)}(0) \\ w^{(n)}(1) \\ \vdots \\ w^{(n)}(L-1) \end{bmatrix} + \mu e(n) \begin{bmatrix} r(n) \\ r(n-1) \\ \vdots \\ r(n-L+1) \end{bmatrix} \tag{10}$$

where μ is an adjustable step size parameter that controls convergence and steady state error variance [21]. Detection then proceeds as described in the context of the detector in Figure 1.

B. Equalization Based on Decision Feedback Minimum Mean Squared Error

Equalization based on the decision feedback minimum mean squared error criterion for offset QPSK was developed by Tu [10]. The LMS adaptive version, illustrated in Figure 2 (b), is described as follows. The detection filter output $z_d(t)$ is sampled at two samples/symbol. The n-th sample is filtered by the FIR feedforward filter with L_{FF} coefficients $w_{\text{FF}}^{(n)}(k)$ $(k = -(L_{\text{FF}}-1)/2, \ldots, (L_{\text{FF}}-1)/2)$ at time index n. The output of the feedforward filter, $z_{\text{FF}}(n)$ is given by

$$z_{\text{FF}}(n) = \sum_{l=-\frac{L_{\text{FF}}-1}{2}}^{\frac{L_{\text{FF}}-1}{2}} w_{\text{FF}}^{(n)}(l) z_d(n-l). \tag{11}$$

This output is combined with the output of the length-L_{FB} feed back filter, z_{FB} to form the signal $z(n) = z_{\text{FF}}(n) + z_{\text{FB}}(n)$. The output of the feedback filter is given by

$$z_{\text{FB}} = \sum_{l=0}^{L_{\text{FB}}-1} w_{\text{FB}}^{(n)}(l) D(n-l) \tag{12}$$

where $w_{\text{FB}}^{(n)}(l)$ is the l-th coefficient of the feedback filter at time index n and $D(n)$ is based on the decisions. Due to the offset nature of the modulation, symbol decisions are based on samples that alternate between the real and imaginary parts of the feed forward filter output. Assuming the even-indexed samples correspond to the data sample on the real component and the odd-indexed samples correspond to the data on the imaginary component, $D(n)$ may be expressed as

$$D(n) = \begin{cases} \Re\left\{\hat{d}(k)\right\}, \Im\left\{\hat{d}(k-1)\right\}, \Re\left\{\hat{d}(k-1)\right\}, \ldots \\ \qquad \text{for } n \text{ even and } k = \dfrac{n}{2} \\ \Im\left\{\hat{d}(k)\right\}, \Re\left\{\hat{d}(k)\right\}, \Im\left\{\hat{d}(k-1)\right\}, \ldots \\ \qquad \text{for } n \text{ odd and } k = \dfrac{n-1}{2} \end{cases} \tag{13}$$

where the decision are

$$\hat{d}(k) = \begin{cases} \text{sgn}\left(\Re\left\{z\left(\frac{n}{2}\right)\right\}\right) & n \text{ even} \\ j\,\text{sgn}\left(\Im\left\{z\left(\frac{n-1}{2}\right)\right\}\right) & n \text{ odd} \end{cases}. \tag{14}$$

The alternating nature of the error signal is the key difference between the MMSE equalization algorithm for offset modulations and non-offset modulations.

The feedforward and feedback filter coefficient updates can be realized using any of the standard adaptive filter techniques such as LMS (and its variants) or RLS [21]. Using the LMS

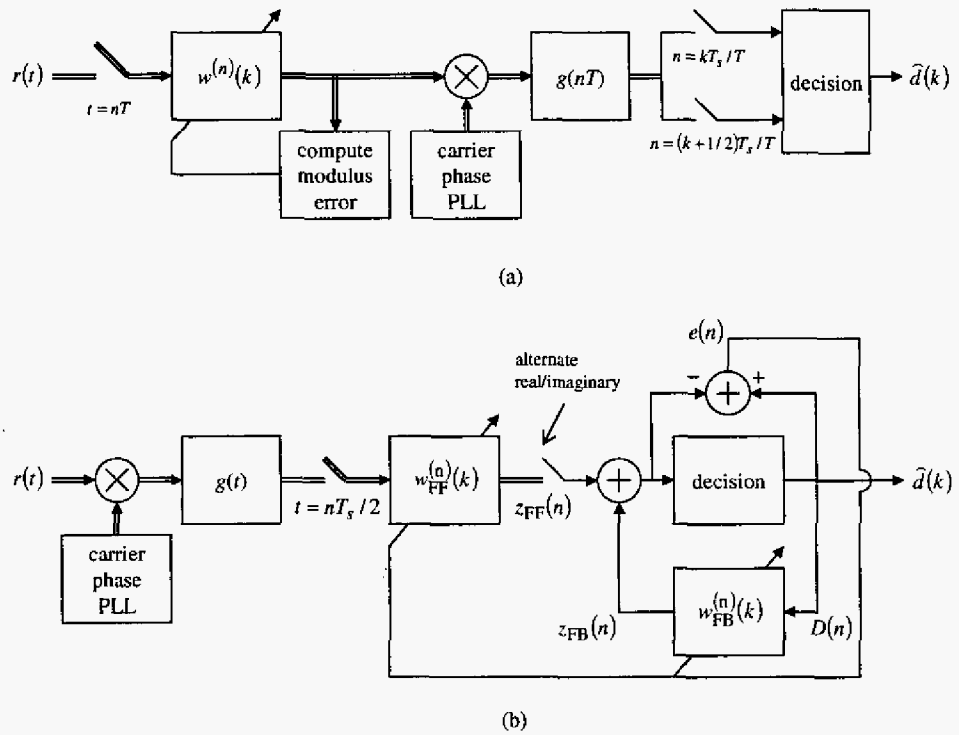

Fig. 2. Adaptive equalization algorithms suitable for FQPSK and SOQPSK: (a) CMA equalizer; (b) DF-MMSE equalizer.

algorithm, the update equations are

$$\begin{bmatrix} w_{\mathrm{FF}}^{(n+1)}\left(-\frac{L_{\mathrm{FF}}-1}{2}\right) \\ \vdots \\ w_{\mathrm{FF}}^{(n+1)}(0) \\ \vdots \\ w_{\mathrm{FF}}^{(n+1)}\left(\frac{L_{\mathrm{FF}}-1}{2}\right) \end{bmatrix} = \begin{bmatrix} w_{\mathrm{FF}}^{(n)}\left(-\frac{L_{\mathrm{FF}}-1}{2}\right) \\ \vdots \\ w_{\mathrm{FF}}^{(n)}(0) \\ \vdots \\ w_{\mathrm{FF}}^{(n)}\left(\frac{L_{\mathrm{FF}}-1}{2}\right) \end{bmatrix} + \mu e(n) \begin{bmatrix} z_d^*\left(n+\frac{L_{\mathrm{FF}}-1}{2}\right) \\ \vdots \\ z_d^*(n) \\ \vdots \\ z_d^*\left(n-\frac{L_{\mathrm{FF}}-1}{2}\right) \end{bmatrix} \tag{15}$$

$$\begin{bmatrix} w_{\mathrm{FB}}^{(n+1)}(0) \\ w_{\mathrm{FB}}^{(n+1)}(1) \\ \vdots \\ w_{\mathrm{FB}}^{(n+1)}(L_{\mathrm{FB}}-1) \end{bmatrix} = \begin{bmatrix} w_{\mathrm{FB}}^{(n)}(0) \\ w_{\mathrm{FB}}^{(n)}(1) \\ \vdots \\ w_{\mathrm{FB}}^{(n)}(L_{\mathrm{FB}}-1) \end{bmatrix} + \mu e(n) \begin{bmatrix} D^*(n) \\ D^*(n-1) \\ \vdots \\ D^*(n-L+1) \end{bmatrix} \tag{16}$$

where μ is the adjustable step size. The numerical results summarized in the next section use the LMS algorithm.

IV. Performance

The performance of both FQPSK and SOQPSK-TG using both the CMA and the DF-MMSE equalizers were simulated in the presence of multipath interference typical of that encountered in aeronautical telemetry [8]. The multipath interference can be modeled as an linear system with impulse response

$$h(t) = \delta(t) + \Gamma_1\delta(t-\tau_1) + \Gamma_2\delta(t-\tau_2). \tag{17}$$

The first multipath component with complex amplitude Γ_1 and delay τ_1 is a result of a strong "ground bounce" off the dry lake beds typical of test ranges in the Western USA. These parameters are a function of the system geometry (i.e. the relative locations of the airborne transmitter and the receiver ground station). $|\Gamma_1|$ can be as large as 0.8 or 0.9 and the delay is typically in the 40–80 ns range. At 20 Mbits/sec, this delay is on the order of half a symbol time. The second multipath component with amplitude Γ_2 and delay τ_2 is due to reflections from irregular terrain. As a consequence, the multipath component is much more random with $|\Gamma_2|$ on the order of 0.01 and τ_2 on the order of a few hundred ns.

In the simulations that follow, the channel impulse response is

$$h(t) = \delta(t) + |\Gamma_1|e^{j\pi}\delta\left(t-0.5T_s\right). \tag{18}$$

The phase of Γ_1 is set to π to produce the worst multipath interference. $|\Gamma_1|$ was varied from 0.1 to 0.8 to monitor the effect of the relative strength of the multipath interference. The simulations with the DF-MMSE equalizer used the following parameters:

- $L_{\mathrm{FF}} = 21$, $L_{\mathrm{FB}} = 18$ (at 2 samples/symbol, the filters spanned 19.5 symbols or 39 bits).
- training length = 3000 bits
- LMS step size $\mu = 10^{-3}$

The simulations using the CMA equalizer used the following parameters:

- $N = 10$ samples/symbol
- $L = 195$ (the filter spans 19.5 symbols or 39 bits)
- filter tap initialization period = 3000 bits
- LMS step size $\mu = 10^{-5}$

The simulation results for FQPSK are shown in Figures 3, 4, and 5. Figure 3 is a plot of the bit error rate performance

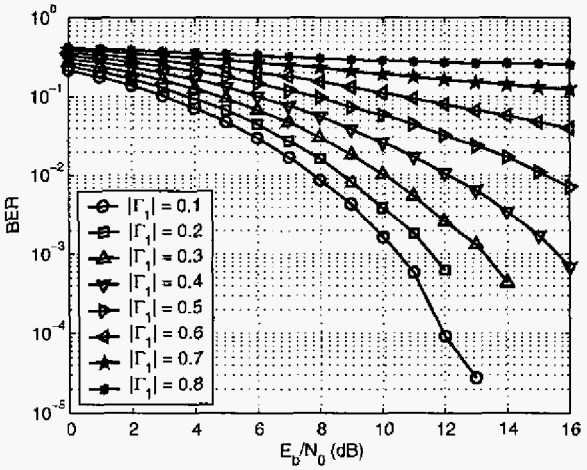

Fig. 3. Performance of unequalized FQPSK on the channel 18.

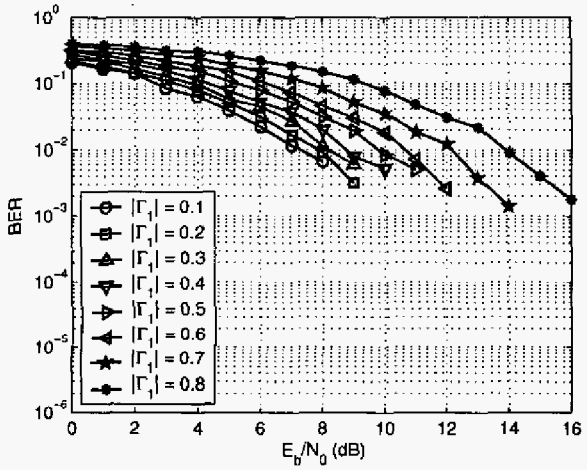

Fig. 4. Performance of FQPSK using the CMA equalizer on the channel 18.

of unequalized FQPSK and is included for reference. A comparison of the bit error rate for FQPSK using CMA equalization (Figure 4) and DF-MMSE equalization (Figure 5) shows that DF-MMSE equalizer seems to perform a little better than the CMA equalizer, although both improve the bit error rate performance. The performance improvement is more pronounced as $|\Gamma_1|$ increases.

The simulation results for SOQPSK-TG are shown in Figures 6, 7, and 8. Figure 6 is a plot of the bit error rate performance of unequalized SOQPSK-TG and is included for reference. A comparison of the bit error rate for SOQPSK-TG using CMA equalization (Figure 4) and DF-MMSE equalization (Figure 5) shows that DF-MMSE equalizer seems to perform a litter better than the CMA equalizer, similar to the characteristic observed for FQPSK.

V. Discussion and Conclusions

While both CMA and DF-MMSE equalizers are able to reduce the performance loss due to multipath interference to acceptable levels, there are implementation differences that

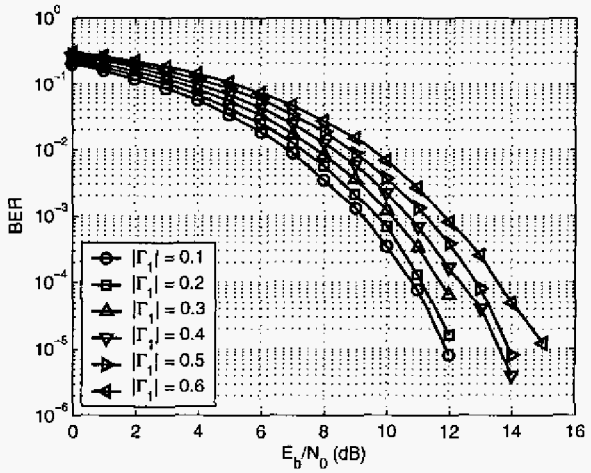

Fig. 5. Performance of FQPSK using the DF-MMSE equalizer on the channel 18.

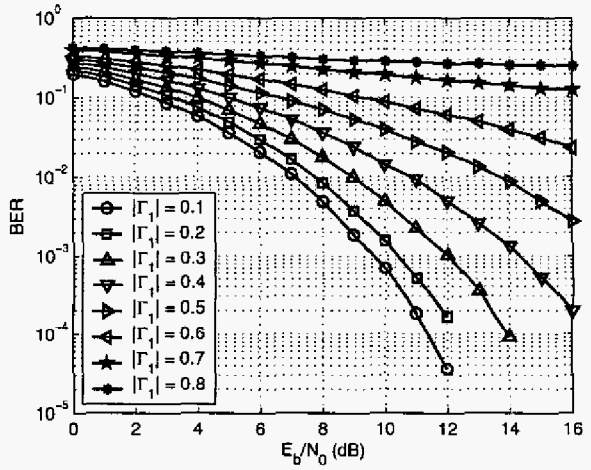

Fig. 6. Performance of unequalized SOQPSK-TG on the channel 18.

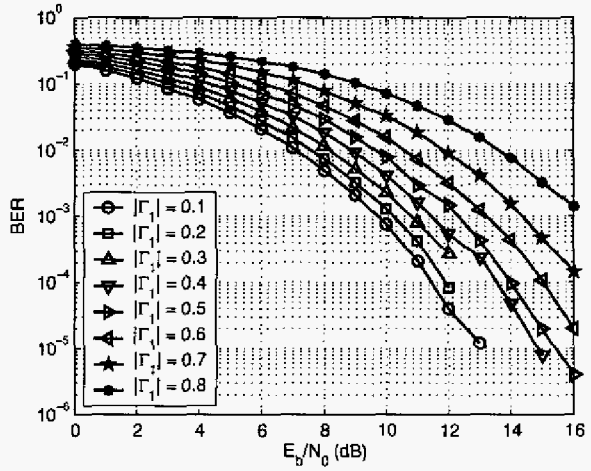

Fig. 7. Performance of SOQPSK-TG using the CMA equalizer on the channel 18.

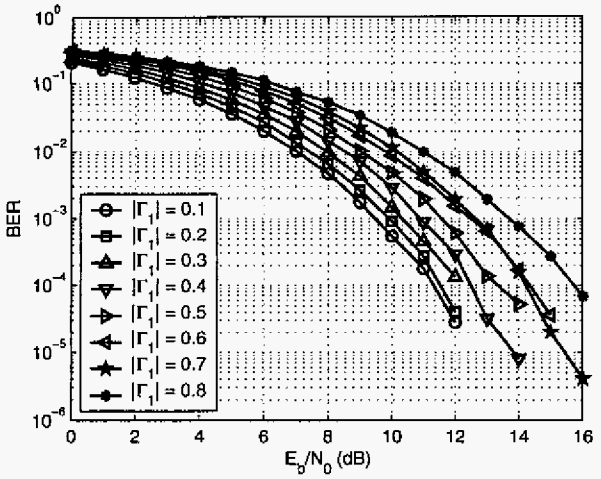

Fig. 8. Performance of SOQPSK-TG using the DF-MMSE equalizer on the channel 18.

should be noted. Both equalizers were chosen to span the same number of bit intervals. Since the DF-MMSE equalizer operates at two samples/symbol, it requires fewer multiplies than the CMA equalizer. The number of CMA filter coefficients would be the same as the number of filter coefficients for the DF-MMSE equalizer if the CMA equalizer could operate at two samples/symbol. However simulation results (not included due to space limitations) show significant performance degradations when the detection filter operates at 2 samples/symbol. These same results suggest $N = 10$ samples/symbol produces nearly optimum results. Thus, for the ARTM Tier-1 waveforms, the CMA equalizer will require more filter coefficients than the DF-MMSE equalizer.

The CMA equalizer is truly blind; it does not require knowledge of the data symbols, carrier phase, or timing synchronization to operate. This is an attractive feature since multipath interference often makes it difficult to obtain accurate estimates of the carrier phase and symbol timing. The DF-MMSE requires a known training sequence, at least from a "cold start". Simulation results with carrier phase offset also show that the DF-MMSE equalizer requires at least course carrier phase synchronization to achieve acceptable performance. Normally, DF-MMSE equalizers also require symbol timing and it is common knowledge that fractionally spaced equalizers are less susceptible to symbol timing errors than symbol-spaced equalizers [9]. However, if the feedforward filter is long enough, the DF-MMSE equalizer is still able to function. The feedforward filter adapts to a filter that compensates for the multipath interference and performs the interpolations to adjust for the timing error. In the simulations performed for this paper, the $L_{FF} = 21$ is long enough to compensate for a timing error up to half a symbol time.

In conclusion, the CMA and DF-MMSE equalizers are able to compensate for the multipath interference encountered in aeronautical telemetry applications. These two equalizers present slight performance/complexity trade-offs than can be exploited to advantage. For both the waveforms, the DF-MMSE equalizer provided slightly better bit error rate performance than the CMA equalizer. This is somewhat expected since the CMA equalizer is completely blind while the DF-MMSE equalizer is not. The CMA equalizer requires a longer adaptive filter and must operate at a higher clock rate than the DF-MMSE equalizer, but the DF-MMSE equalizer requires training and at least course carrier phase synchronization.

REFERENCES

[1] C. Irving, "Range telemetry improvement and modernization," in *Proceedings of the International Telemetering Conference*, Las Vegas, NV, October 1997, pp. 294 – 303.

[2] W. Gao and K. Feher, "FQPSK: A bandwidth and RF power efficient technology for telemetry applications," in *Proceedings of the International Telemetering Conference*, Las Vegas, NV, October 1997, pp. 480–488.

[3] *IRIG Standard 106-00: Telemetry Standards*, Range Commanders Council Telemetry Group, Range Commanders Council, White Sands Missile Range, New Mexico, 2000, (Available on-line at http://jcs.mil/RCC/manuals/106-00).

[4] T. Hill, "An enhanced, constant envelope, interoperable shaped offset QPSK (SOQPSK) waveform for improved spectral efficiency," in *Proceedings of the International Telemetering Conference*, San Diego, CA, October 2000, pp. 127–136.

[5] E. Law and K. Feher, "FQPSK versus PCM/FM for aeronautical telemetry applications; spectral occupancy and bit error probability comparisons," in *Proceedings of the International Telemetering Conference*, Las Vegas, NV, October 1997, pp. 489–496.

[6] M. Goeghegan, "Description and performance results for the advanced range telemetry (ARTM) tier II waveform," in *Proceedings of the International Telemetering Conference*, San Diego, CA, October 2000, pp. 90–96.

[7] T. Hill, "Performance of SOQPSK and multi-h CPM in the presence of adjacent channel interference," in *Proceedings of the International Telemetering Conference*, Las Vegas, NV, October 2001, pp. 255–263.

[8] M. Rice, A. Davis, and C. Bettwieser, "A wideband channel model for aeronautical telemetry," *IEEE Transactions on Aerospace and Electronic Systems*, vol. 40, no. 1, pp. 57–69, January 2004.

[9] J. Proakis, *Digital Communications*. McGraw-Hill, 2001.

[10] J. Tu, "Optimum MMSE equalization for staggered modulation," in *Proceedings for the IEEE Asilomar Conference on Signals, Systems, and Computers*, vol. 2, Asilomar, CA, November 1993, pp. 1401–1406.

[11] K. Feher and S. Kato, U. S. Patent 4,567,602; K. Feher, U. S. Patent 5,491,457; K. Feher, U.S. Patent 5,784,402.

[12] S. Kato and K. Feher, "XPSK: A new cross-correlated phase-shift-keying modulation technique," *IEEE Transactions on Communications*, vol. 31, no. 5, pp. 701 –707, May 1983.

[13] M. Simon, *Bandwidth-Efficient Digital Modulation with Application to Deep Space Communications*. Wiley-Interscience, 2003.

[14] J. Anderson, T. Aulin, and C.-E. Sundberg, *Digital Phase Modulation*. New York: Plenum Press, 1986.

[15] A. Svensson and C.-E. Sundberg, "Optimum MSK-type receivers for CPM on Gaussian and Rayleigh fading channels," *IEE Proceedings*, pp. 480–490, August 1984.

[16] ——, "Serial MSK-type detection of partial response continuous phase modulation," *IEEE Transactions on Communications*, vol. 33, no. 1, pp. 44–52, January 1985.

[17] M. Geoghegan, "Optimal linear detection of SOQPSK," in *Proceedings of the International Telemetering Conference*, San Diego, CA, October 2002.

[18] D. Godard, "Self-recovering equalization and carrier tracking in two-dimensional data communications systems," *IEEE Transactions on Communications*, vol. 28, no. 11, pp. 1867–1875, November 1980.

[19] J. Treichler and B. Agee, "A new approach to multipath correction of constant modulus signals," *IEEE Transactions on Acoustics, Speech, and Signal Processing*, vol. 31, no. 2, pp. 459–472, April 1983.

[20] J. Treichler and M. Larimore, "New processing techniques based on the constnat modulus adaptive algorithm," *IEEE Transactions on Acoustics, Speech, and Signal Processing*, vol. 33, no. 2, pp. 420–431, April 1985.

[21] S. Haykin, *Adaptive Filter Theory*. Prentice-Hall, 2001.